Fast Growth and Sheared Flow Generation in Nonlinear Development of Double Tearing Modes

J. Q. Dong[1,2], Y. X. Long[1], Z. Z. Mou[1], Z.X. Wang[3], J.Q. Li[2,3], Y. Kishimoto[3]

1, Southwestern Institute of Physics, P.O. Box 432, Chengdu, China
2, Institute for Fusion Theory and Simulation, Zhejiang University, Hangzhou, China
3, Department of Fundamental Energy, Kyoto University, 611-0011 Gokasho, Uji, Japan

e-mail:jiaqi@swip.ac.cn

Abstract The nonlinear development of double tearing modes (DTMs) mediated by parallel electron viscosity in a large aspect ratio torus is simulated. The emphasis is placed on the mechanisms for the fast growth and sheared flow generation in the development of the DTMs. Four nonlinear developing stages: the early growth, transition, fast growth and decay, are found. In comparison with the helical magnetic flux contour, the fast growth is revealed to be associated with the reconnection and annihilation of the magnetic islands formed by the reconnection of equilibrium magnetic field in early stage of the mode development. The quantitative scaling of the growth rate and the flow shear with respect to electron viscosity is presented. The stabilization effect of a vortex flow generated in tearing mode development on ion temperature gradient modes is also demonstrated stronger than that of a mean or streamer flow of same magnitude.

1. Introduction

A non-monotonic safety factor q profile is desirable for advanced tokamak (AT) operation with internal transport barriers (ITBs). The latter are formed preferentially in proximities of low safety factor q rational flux surfaces and often coincide with occurrence of magnetohydrodynamics (MHD) activities in experiments [1-6]. The double tearing modes (DTMs) are known to develop preferentially around the surface of minimum q close to a rational value. On the other hand, ITB formation is commonly accepted as a result of turbulence suppression by sheared flows in AT discharges [7-9]. Therefore, the relation between low q rational flux surfaces, MHD activities, flow layer formation, turbulence suppression, and ITB formation is essential for understanding the experiments. The interaction between MHD activities and transport inducing turbulence, in general, and possible causal relationship between DTM and the ITB triggering, in particular, is one of research focuses [9-12]. In addition, characteristics of nonlinear DTMs are important for understanding tokamak plasma behaviors in discharges with negative magnetic shear (NMS) [13, 14]. The nonlinear fast growth and flow layer formation in development of DTMs and single tearing mode (STM) have been studied in slab geometry [15-19]. The fast growth and flow layer formation in nonlinear development of DTMs is studied for large aspect ratio toroidal plasmas in this work. The mechanisms for the fast growth and sheared flow generation in the mode development are investigated in detail. The effects of the sheared helical or vortex flows, formed in the tearing mode development, on the ion temperature gradient modes (ITG) are also investigated in a sheared slab.

2. Physics model and basic equations

We consider a large aspect ratio torus with a major radius R_0 and minor radius a. A cylindrical coordinate (r,θ,φ) is employed. The magnetic field and plasma velocity are expressed in terms of two scalar potentials: the poloidal flux function $\psi(r,\theta,\varphi)$,

$$\vec{B} = B_0\vec{\varphi} - \nabla\psi\times\vec{\varphi}, \tag{1}$$

and the stream function $\phi(r,\theta,\varphi)$,

$$\vec{V} = v_0\vec{\varphi} + \nabla\phi\times\vec{\varphi}. \tag{2}$$

With electron viscosity included, the Ohm's law becomes

$$\vec{E} = \eta\vec{j} - \frac{1}{c}\vec{v}\times\vec{B} - \frac{m_e\mu_e}{n_e e^2}\nabla^4\vec{j}. \tag{3}$$

Using Faraday's law and Eq.(1), it is straightforward to get

$$\frac{\partial\psi}{\partial t} = -\vec{v}\cdot\nabla\psi + \frac{\eta c^2}{4\pi}\nabla^2\psi - \frac{m_e\mu_e c^2}{4\pi n_e e^2}\nabla^4\psi + E_w - \frac{B_0}{R_0}\frac{\partial}{\partial\varphi}\phi \tag{4}$$

from the φ-component of Eq.(3). Here, η is the plasma resistivity, μ_e is the parallel electron viscosity diffusion coefficient, m_e is electron mass, n_e is electron density, and e and c are, respectively, the electron charge and speed of light, B_0 is the toroidal magnetic field at the magnetic axis, and v_0 is equilibrium toroidal velocity.

The φ-component of the curl of the equation of plasma motion may be written as

$$\frac{\partial}{\partial t}(\nabla^2{}_\perp\phi) = -(\vec{v}\cdot\nabla_\perp)\nabla^2{}_\perp\phi - \frac{v_0}{\rho}\frac{\partial}{R_0\partial\varphi}\nabla^2{}_\perp\phi + \frac{1}{4\pi\rho}[\nabla^2{}_\perp(\nabla^2{}_\perp\psi)\times\nabla_\perp\psi]\cdot\vec{\varphi} - \frac{\mu}{\rho}\nabla^4{}_\perp\phi \tag{5}$$

where ρ is the plasma mass density and μ is the fluid viscosity. Then, the basic governing reduced MHD (RMHD) equations are derived from Eqs. (1), (4) and (5) as

$$\frac{\partial\psi}{\partial t} = -[\psi,\phi] - \frac{B_0}{R_0}\frac{\partial\phi}{\partial\varphi} + S^{-1}\nabla^2_\perp\psi - R_e^{-1}\nabla^2_\perp\chi + E_w, \tag{6}$$

$$\frac{\partial}{\partial t}(\nabla^2_\perp\phi) = -[U,\phi] - \frac{v_0}{R_0}\frac{\partial U}{\partial\varphi} + [\nabla^2_\perp\psi,\psi] - \frac{B_0}{R_0}\frac{\partial\nabla^2_\perp\psi}{\partial\varphi} + \frac{1}{R_i}\nabla^2_\perp U. \tag{7}$$

Here, $\chi = \nabla^2_\perp\psi$, $U = \nabla^2_\perp\phi$, and the Laplacian and Poisson bracket are defined as,

$$\nabla^2_\perp = \frac{\partial^2}{\partial r^2} + \frac{1}{r}\frac{\partial}{\partial r} + \frac{1}{r^2}\frac{\partial^2}{\partial\theta^2}, \quad (8) \qquad \text{and} \qquad [a,b] = \frac{1}{r}\left(\frac{\partial a}{\partial r}\frac{\partial b}{\partial\theta} - \frac{\partial b}{\partial r}\frac{\partial a}{\partial\theta}\right). \tag{9}$$

The usual normalizations are employed such that lengths are normalized to a, magnetic fields are to $B_\theta(a)$, time is to $\tau_{pa} = a\sqrt{4\pi\rho}/B_\theta(a)$ etc. In addition, $S = \tau_r/\tau_{pa}$ is the magnetic Reynolds number with $\tau_r = 4\pi a^2/\eta c^2$ being the magnetic diffusion time, $R_e = \tau_v/\tau_{pa}$ is the viscosity diffusion Reynolds number, while $\tau_v = 4\pi n_e{}^2 a^4 e^2/m_e\mu_e c^2$ is the electron viscosity diffusion time, and $R_i = \tau_i/\tau_{pa}$ with $\tau_i = \rho a^2/\mu_i$.

3. Fast growth and velocity Shear layer formation

The equilibrium configuration with non-monotonic q profile is employed [14],

$$q(r) = q_c\{1+(\frac{r}{r_0})^{2\lambda}\}^{1/\lambda}[1+A\exp\{-(\frac{r-r_\delta}{\delta})^2\}], \quad \psi_{0,0}(r) = -\frac{B_0}{R_0}\int_0^r \frac{rdr}{q(r)}, \quad s(r) = \frac{r}{q(r)}\frac{dq(r)}{dr}.$$

The parameters are chosen such q_c=1.05, $\lambda = 1, r_0 = 0.412$, $\delta = 0.273, r_\delta = 0, A = 3$ that two resonant q=3 surfaces are located at r_1=0.31 and r_2=0.53. $v_0 = 0$ is assumed.

The numerical code for solving the nonlinear partial differential equations (6, 7) is benchmarked with an eigenvalue code in the linear stage and with the results in [14] for nonlinear simulations. The eigenfunctions from the eigenvalue code, with the lowest m and n, multiplied with a small factor, are taken as the initial conditions. The initial values for the other components are all taken to be zero. The boundary conditions are that the perturbations and their radial derivatives are zero at the center (r=0) and the plasma boundary (r=1). The maximum 2000 grid points are employed in the radial direction and the results are checked to be independent of the number of the grid points.

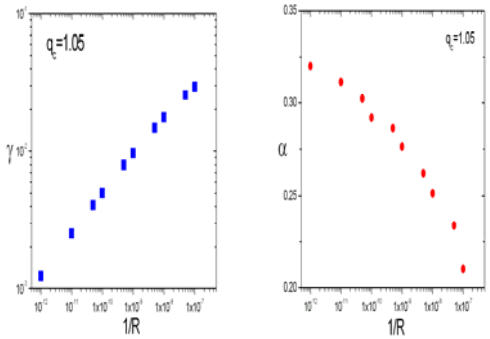

Fig. 1. The linear growth rate and the scaling index α of $\gamma \propto R^{-\alpha}$ versus 1/R.

The DTMs mediated by electron viscosity are studied. Shown in Fig. 1 are the linear growth rate and the scaling index α of $\gamma \propto R^{-\alpha}$ versus 1/R. The transition from the scaling of $\gamma \propto R^{-1/3}$ to $\gamma \propto R^{-1/5}$ is clearly demonstrated for increasing 1/R [15].

The time evolution of the perturbed total kinetic and magnetic energies for R=5×10^6, 10^7, 5×10^7 and 10^8, and of energies of the lowest seven harmonics for R=10^8 is given in Fig.2. After a short linear growth, the total perturbed kinetic energy goes through four developing stages: the early growth, transition, fast growth and decay when R$\geq 5\times10^7$ in contrast to the cases of R$\leq 10^7$ where there are no fast growth stages. In addition, there are no fast growth stages in the perturbed

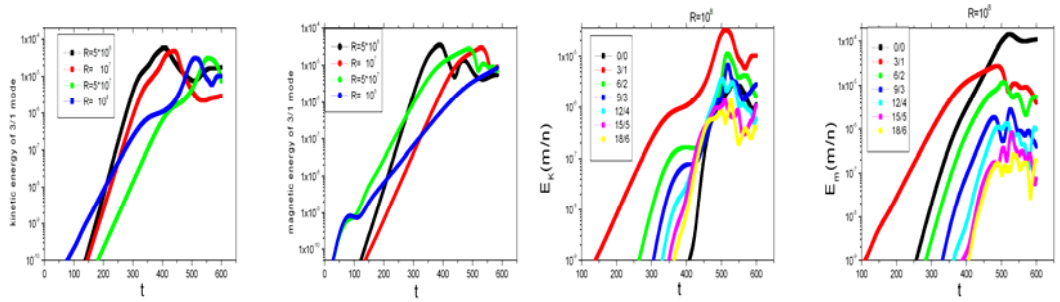

Fig.2, The time evolutions of the perturbed total kinetic and magnetic energies for R=5×10^6, 10^6, 5×10^7 and 10^8, and the energies of the first seven harmonics for R=10^8.

magnetic energy either. The harmonic analysis indicates that the fast growth is dominated by the m=3/n=1 harmonic but may be relevant with the appearance of the higher harmonics at the transition stage. The appearance around t=250 and significant growth of

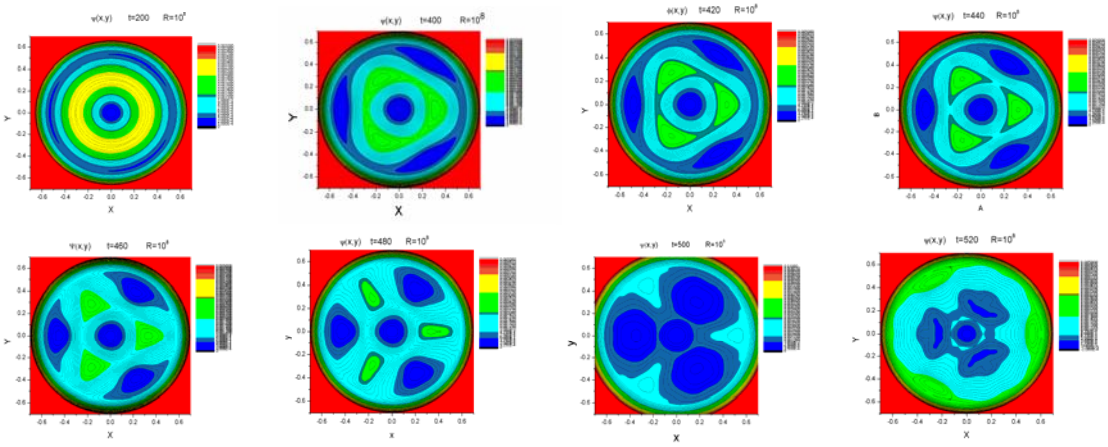

Fig. 3. *The helical magnetic flux contours at t=200, 400, 420, 440, 460, 480, 500, and 520.*

the m=0/n=0 magnetic perturbation, which induces variation of the equilibrium magnetic configuration, seem to be the cause of the transition or transient saturation. Shown in Fig. 3 are the contours of the helical magnetic flux at t=200, 400, 420, 440, 460, 480 500, and 520 for $R=10^8$. There are two chains of magnetic islands located at the two q= 3 rational surfaces before t=400. The magnetic islands grow rather fast with the inner and outer chains moving outwards and inwards, respectively. The islands of the two chains start to reconnect with each other after the flux between them is all reconnected out due to the fact that the fluxes inside the two chains are opposite to each other. It is this secondary reconnection and the annihilation of the magnetic islands formed in the first reconnection of equilibrium magnetic field in the early development of the mode that is responsible for the fast growth of the kinetic energy from t=450 to 500. The m=0/n=0 magnetic perturbation is saturated and the higher harmonics start decay after t=500.

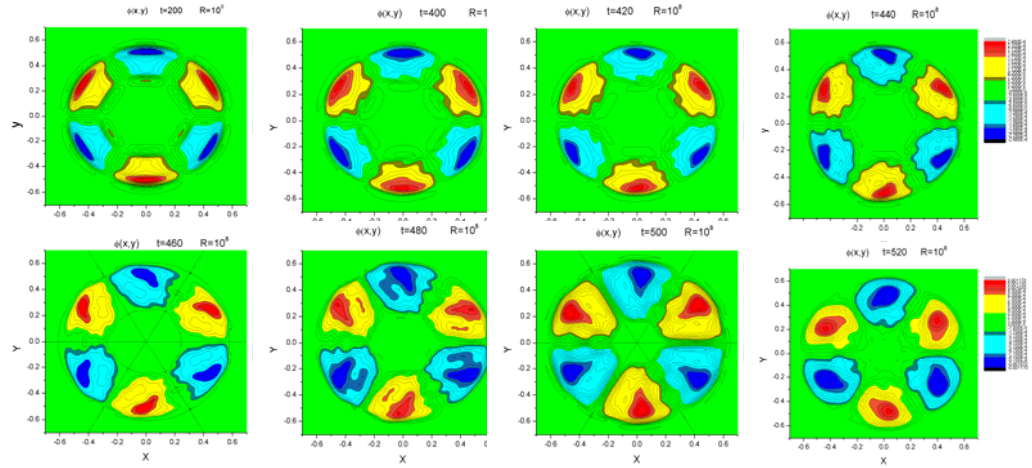

Fig.4. *The stream function contours at t=200, 400, 420, 440, 460, 480, 500, and 520.*

The contours of the stream function at t=200, 400, 420, 440, 460, 480, 500, and 520 are given in Fig.4 for $R=10^8$. There is not an apparent two chain structure, illustrating the approximate constant displacement amplitude of the DTM over the region between the two rational surfaces. In addition, the flow and is shear are mainly confined in the

vicinity of the r_2=0.53 rational surface for $t \le 420$ when the magnetic islands keep growing. The contours begin distortion when the two island chains start to reconnect with each other and to annihilate. To see this more clearly, the profiles of the amplitudes of the m=3/n=1 harmonic of the stream function ϕ (a), the velocity v_θ (b) and its radial gradient (c) are given in Fig. 5. It is clearly shown that significant m=3/n=1 harmonic velocity and its shear appear around the two resonant flux surfaces at t=300 and then grow very fast. In comparison, the amplitude of the m=6/n=2 harmonic given in Fig. 5(d) is more than one order of magnitude smaller than that of the m=3/n=1 harmonic. This is an important indicator that the flow with the largest poloidal scale length dominates in the entire process, especially in the early stage, of the mode development.

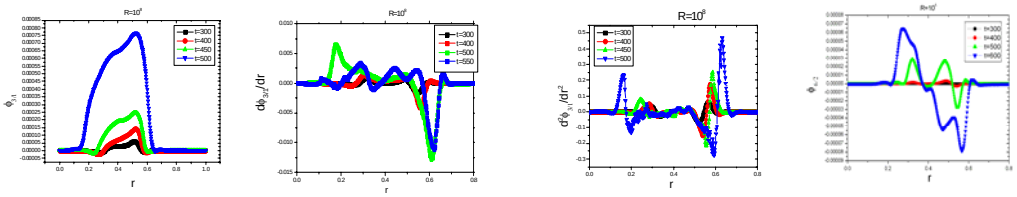

Fig. 5. The profiles of the amplitude of the m=3/n=1 harmonic of the stream function (a), the velocity (b) and its shear (c), and the profile of the amplitude of the m=6/2=1harmonic of the stream function (d).

Shown in Fig. 6 are the amplitude profiles of the m=3/n=1 harmonic of the poloidal flux function, the extensions of which are equivalent to the profiles of the perturbed radial magnetic field and relevant to the widths of the magnetic islands. Keeping this in mind and in comparison with Fig. 5, it is rather evident that the flow shear layers are mostly confined in the regions just outside the magnetic islands. This is an inevitable result due to the facts that magnetic energy released in nonlinear development of the modes converts to kinetic energy and the coherent plasma motion, perpendicular to magnetic field, is prohibited in ideal MHD region, and, therefore, is confined in the tearing layer.

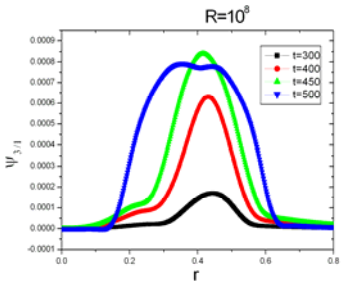

Fig. 6. The amplitude profiles of the m=3/n=1 harmonic of the poloidal flux function.

4. Effects of helical flow on ion temperature gradient modes

Self-consistent study of the effects of the helical sheared flow and magnetic islands spontaneously generated in the development of tearing modes on micro-instability and turbulence is a big challenge. The effects of a helical flow on ITG modes, neglecting magnetic island structures, are discussed in a sheared slab as the first step in this Section. The helical flows reduce to vortex flows (VFs) in the slab. The VF is considered static and expressed with the stream function,

$$\phi_T = \phi_{TX}(x)\sin(k_T y) = \phi_m f(x)\sin(k_T y), \qquad (10)$$

where $f(x)$ is the normalized radial profile of the VF and k_T is its poloidal wave vector. ϕ_m is the amplitude.

The nonlinear electrostatic gyrofluid model in a 2-dimensional (2D) slab ($\partial_z = 0$) is

employed with the above external VF included [20],

$$\frac{\partial V^{k_y}}{\partial t} = (1+K\nabla_\perp^2)\frac{\partial \phi^{k_y}}{\partial y} + \nabla_\parallel v_\parallel^{k_y} - [\phi^{k_y'}, \nabla_\perp^2 \phi^{k_y''}] + \mu_\perp \nabla_\perp^4 \phi^{k_y} + \frac{\partial \phi^{k_y}}{\partial y}\frac{\partial \bar{\phi}}{\partial x}$$
$$-\frac{i}{2}\phi_m \frac{\partial f(x)}{\partial x}[ik_y''' V^{k_y''} - ik_y'' V^{k_y'''}] - \frac{i}{2}(ik_T)\phi_m f(x)\left(\frac{\partial V^{k_y'''}}{\partial x} + \frac{\partial V^{k_y''''}}{\partial x}\right), \quad (11)$$

$$\frac{\partial v_\parallel^{k_y}}{\partial t} = -\nabla_\parallel(\phi^{k_y} + p^{k_y}) - [\phi^{k_y'}, v_\parallel^{k_y''}] + \eta_\perp \nabla_\perp^2 v_\parallel^{k_y}$$
$$-\frac{i}{2}\phi_m \frac{\partial \phi_m f(x)}{\partial x}[ik_y''' v_\parallel^{k_y''} - ik_y'' v_\parallel^{k_y'''}] - \frac{i}{2}(ik_T)\phi_m f(x)\left(\frac{\partial v_\parallel^{k_y'''}}{\partial x} + \frac{\partial v_\parallel^{k_y''''}}{\partial x}\right), \quad (12)$$

$$\frac{\partial p^{k_y}}{\partial t} = -K\frac{\partial \phi^{k_y}}{\partial y} - \Gamma\nabla_\parallel v_\parallel^{k_y} - (\Gamma-1)\sqrt{\frac{8}{\pi}}|k_\parallel|(p^{k_y} - \phi^{k_y}) - [\phi^{k_y'}, p^{k_y''}] + \chi_\perp \nabla_\perp^2 p^{k_y}$$
$$-\frac{i}{2}\phi_m \frac{\partial f(x)}{\partial x}[ik_y''' p^{k_y''} - ik_y'' p^{k_y'''}] - \frac{i}{2}(ik_T)\phi_m f(x)\left(\frac{\partial p^{k_y'''}}{\partial x} + \frac{\partial p^{k_y''''}}{\partial x}\right), \quad (13)$$

where, $k_y' + k_y'' = k_y''' + k_T = k_y'''' - k_T = k_y$, $K = 1+\eta_i$ and $V^{k_y} = (\nabla_\perp^2 + \delta - 1)\phi^{k_y}$, $\delta = 1\,(0)$ for zonal flow (fluctuating components). The notation and normalization as well as the magnetic configuration are the same as that in [20]. This set of mode coupling equations derived in the same way as that in [20] clearly shows the interaction between a VF and ITG modes through both radial and poloidal couplings by the last two terms on the right hand side (RHS) of each equation.

The Equations (11)-(13) are numerically solved by using of a 2D initial value code. The simulation box is $L_x = 100\rho_i$ and $L_y = 20\pi\rho_i$. Fixed and periodic boundary conditions are imposed at $x = \pm\frac{1}{2}L_x$ and y=0, L_y, respectively. The other parameters are $\eta_i = 2.2$, $\mu_\perp = \eta_\perp = \chi_\perp = 0.1$, and $k_T = 0.1$. The representative structure of the VF with two vortices on each side of the rational surface, generated in development of a single tearing mode, is shown in Fig. 7. Besides the VF, a streamer-like flow (SF) of $\phi_T = \phi_m \sin(k_T y)$ and a mean flow (MF) of $\phi_T = \phi_m f(x)$ are introduced in helping to understand the complicated stabilization mechanisms of the VF with comparison. Fig. 8 shows the effects of the three external flows on the ITG mode linear growth rate for different magnetic shears, $s = L_n / L_s$. The growth rate increases first and then decreases when the amplitude of the MF increases for the three cases as is well documented [20]. The stabilization effect

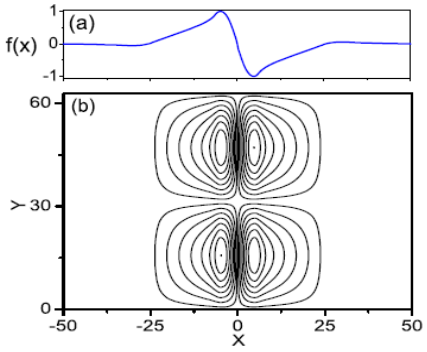

Fig. 7. The radial profile *f(x)* of the stream function $\phi_T = \phi_m f(x)\sin(k_T y)$ (a) and

of the SF decreases dramatically with decreasing magnetic shear.

The effect of the VF is the strongest and the mechanism is relatively complicated. As indicated in Eqs. (13-15), a MF, dependent on *x*, couples a mode to other modes of different radial scale lengths through the first term of the last two terms on the RHS of each equation. Whereas a SF, dependent on *y*, couples a mode to other modes of different poloidal wave vector k_y's through the second term of the last two terms on the RHS of each equation. Generally speaking, coupling to more unstable modes increases the growth rate of the unstable mode under consideration and thus the whole coupled system, and vice verse. Spectrum analysis (not shown here) for $\phi_m = 3$ and *s*=0.4 shows that most unstable modes are limited approximately to the regions of $0.1 < k_x < 5$ and $0.3 < k_y < 1.1$ in the wave vector spectra with the maximum growth rate $\gamma = 0.99$ at k_y~0.7 in the absence of any flows. The unstable k_y-spectrum does not change significantly whereas the k_x-spectrum expands to the region of k_x >2.5, where the growth rates of the modes are lower, when there is a MF. The result is the opposite with a SF; the unstable k_x-spectrum does not change significantly while the k_y-spectrum expands to both $0.2 > k_y$ and k_y >1.1 regions, where the growth rates of the modes are lower. In the case of VF, the unstable k_x-spectrum expands to higher k_x region as it does in the case of a MF, whereas the unstable k_y-spectrum expands to both $0.2 > k_y$ and k_y >1.1 regions as it does in the case with a SF. In addition, the both expansions are broader probably due to enhancement of each other. Therefore, the strongest stabilization effects of a VF on ITG modes than those of a MF or a SF of same magnitude in most of the parameter regimes studied are demonstrated and physically understandable.

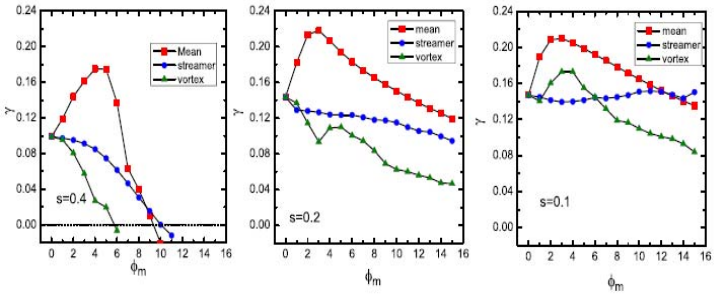

Fig. 8, The linear growth rate of the ITG modes versus the magnitude ϕ_m of the MF, SF and VF (the lines with red squares, blue dots and green triangles), for magnetic shear *s*=0.4, 0.2, and 0.1.

5. **Summary and discussion**

The numerical study of the electron viscosity DTMs and the generation of the helical MHD flows in the development the modes is extended from quasi-linear simulation in a slab [15, 16] to nonlinear simulation in a large aspect ratio torus. The characteristics, such as strong poloidal sheared flows located at the boundaries of the magnetic islands in the nonlinear stage, found in the slab geometry are qualitatively confirmed. Quantitatively speaking, in-out asymmetry of the induced helical velocity profiles is found. The shear at the outer boundary of the islands is higher than that at the inner, in contrast to the slab case [15]. The shear of the velocity was estimated as~10^5/s for $B_\theta(a)$=1.7T, a=0.4m, n_e=10^{19}/m^3 from the numerical results for R=10^8. This is

comparable with the growth rate of the drift instabilities in tokamak plasmas.

As an important part of multi-scale dynamics, the interaction between tearing modes and turbulence is under intensive investigation in plasma physics [10-12]. The subject includes two aspects, the effect of turbulence on tearing modes, and the influence of tearing modes on turbulence and turbulent transport. This is a challenge since it concerns multi- spatial and temporal scales. Physically, a tearing mode consists of two elements: magnetic perturbation, forming magnetic islands, and plasma motion including the helical flows studied in this work. The ultimate aim of the subject is to study the drift wave turbulence dynamics in a realistic toroidal configuration with magnetic islands and plasma flows. Before being able to do so, as a first step, we try to understand the characteristics of the flows and then to put the flows as an input for a turbulence study in a configuration without magnetic islands in this work. The preliminary results show that the stabilization effect on a vortex flow on ITG modes is higher than that of a mean or streamer flow of same magnitude. This may provide insight into the relation between low safety factor q rational surfaces, MHD activities, flow layer and ITB formation in reversed magnetic shear configurations. Works on linear and non-linear development of tearing modes and turbulence self-consistently, taking into account the multi- spatial (from 0.1mm to 0.1m) and temporal (from 0.01 ms to 1ms) scales are in progress.

Acknowledgement

This work is supported by the NSFC Grant No. 10575031 and No. 10575032.

References

[1] Y. Koide *et al*., Phys. Rev. Lett. **72**, 3662 (1994).
[2] C.M. Greenfield et al., Plasma Physics and Controlled Nuclear Fusion Research (IAEA, Vienna, 1998), Vol. 1, P. 13.
[3] M.G. Bell et al., Plasma Phys. Control. Fusion **41**, A719 (1999).
[4] E. Jofrrin et al., Nucl. Fusion **43**, 1167 (2003) and the references therein.
[5] E. Joffrin et al., Nucl. Fusion **42**, 235 (2002).
[6] G.M.D. Hogeweij et al., Plasma Phys. Control. Fusion **44**, 1155 (2002).
[7] P.W. Terry, Rev. Mod. Phys. **72**, 109 (2000).
[8] P. H. Diamond et al., Plasma Phys. Controlled Fusion **47**, R35 (2005).
[9] J.Connor et al., Nucl. Fusion **44**, R1 (2004).
[10] C.J. McDevitt and P.H.Diamond, Phys. Plasmas **13**, 032302 (2006).
[11] Y.Kishimoto et al., Nucl.Fusion **40**, 667(2000).
[12] F. Militello et al., [J] Phys. Plasmas **15**, 050701 (2008).
[13] B. Carreras *et al.*, Phys. Fluids 23(9), 1811-1826(1980).
[14] Y. Ishii, M. Arzumi, G. Kurita, and T. Tuda, Phys. Plasmas **7**, 4477 (2000).
[15] J.Q. Dong, S.M. Mahajan and W. Horton, Phys. Plasmas **10**, 3151 (2003).
[16] J.Q. Dong, Y. X. Long, and Z.Z. Mou *et al.*, Phys. Plasmas **14**, 114501 (2007).
[17] Z. X. Wang, X. G. Wang, and J. Q. Dong *et al.*, Phys. Rev. Lett. **99**, 185004 (2007).
[18] N. F. Loureiro, S. C. Cowly *et al.*, Phys. Rev. Lett. **95**, 235003 (2005).
[19]D. Graso *et al.*, Plasma Phys. & Controlled Fusion **48**, L97 (2006).
[20]] J. Li and Y. Kishimoto, Phys. Plasmas **10**, 683 (2003).